

Geometry-induced spin-filtering in photoemission maps from WTe₂ surface states

Tristan Heider,¹ Gustav Bihlmayer,² Jakub Schusser,^{3,4} Friedrich Reinert,⁴
Jan Minár,³ Stefan Blügel,² Claus M. Schneider,^{1,5,6} and Lukasz Plucinski^{1,*}

¹Peter Grünberg Institut (PGI-6), Forschungszentrum Jülich GmbH, 52428 Jülich, Germany

²Peter Grünberg Institut (PGI-1) and Institute for Advanced Simulation (IAS-1),
Forschungszentrum Jülich and JARA, 52428 Jülich, Germany

³New Technologies-Research Center, University of West Bohemia, 30614 Pilsen, Czech Republic

⁴Experimentelle Physik VII and Würzburg-Dresden Cluster of Excellence ct.qmat, Universität Würzburg, Würzburg, Germany

⁵Fakultät für Physik, Universität Duisburg-Essen, 47048 Duisburg, Germany

⁶Physics Department, University of California, Davis, CA 95616, USA

(Dated: October 21, 2022)

We demonstrate that an important quantum material WTe₂ exhibits a new type of geometry-induced spin-filtering effect in photoemission, stemming from low symmetry that is responsible for its exotic transport properties. Through the laser-driven spin-polarized angle-resolved photoemission Fermi surface mapping, we showcase highly asymmetric spin textures of electrons photoemitted from the surface states of WTe₂. Such asymmetries are not present in the initial state spin textures, which are bound by the time-reversal and crystal lattice mirror plane symmetries. The findings are reproduced qualitatively by theoretical modeling within the one-step model photoemission formalism. The effect could be understood within the free-electron final state model as an interference due to emission from different atomic sites. The observed effect is a manifestation of time-reversal symmetry breaking of the initial state in the photoemission process, and as such it cannot be eliminated, but only its magnitude influenced, by special experimental geometries.

Introduction.—WTe₂ is a semi-metallic two-dimensional (2D) quantum material that exhibits a non-saturating magnetoresistance up to 60 T [1]. It has been debated, whether the bulk electron and hole pockets in WTe₂ slightly overlap leading to the Weyl type-II topological phase [2, 3], with a conjecture that the surface electronic structure would be virtually indistinguishable for a topological and trivial phases [4]. When thinned down to a monolayer, WTe₂ enables the realization of high-temperature quantum Hall phases [5] and gate-controlled superconductivity [6, 7]. In non-magnetic systems the first-order Hall response vanishes at zero magnetic field due to symmetry arguments. However, the second-order correction leads to the recently discovered [8–11] non-linear Hall effect (NLHE) in systems of reduced symmetry. Few-layer WTe₂ has been the first system in which the NLHE has been demonstrated [9, 10] due to the presence of a single mirror plane, and a related existence of polar axes both in-plane and out-of-plane of the layers.

Early high resolution angle-resolved photoemission (ARPES) on WTe₂ [12, 13] have focused on imaging bulk electron and hole pockets with the motivation to explain the non-saturating magnetoresistance, pointing to a possible full charge compensation at lower temperatures. The prediction of possible type-II Weyl states in WTe₂ [2] have further motivated the research on its electronic structure. The reduced symmetry of WTe₂ results in inequivalent top and bottom surfaces along the *c*-axis. The general shape of the experimental WTe₂ band dispersions over the scale of 2 eV below the Fermi level is well reproduced by *ab initio* calculations, however, as pointed out in an early study [12], density functional theory (DFT)

calculations are not able to quantitatively reproduce critical features of the WTe₂ electronic structure near the Fermi level. In particular, this concerns the positions of the electron and hole pockets and related sizes of their Fermi surfaces [14] which play a critical role in understanding the magnetoresistance properties [12, 15]. This lack of agreement, despite occurring on a small energy scale of only 50 meV, is surprising because WTe₂(001) surfaces are clearly very stable under UHV yielding quantitatively consistent results in high-resolution ARPES for the set of dispersive occupied features located near the Fermi level [4, 12–14, 16–18].

Using the newly-developed high resolution laser-driven spin-polarized ARPES (SARPES) spectrometer we demonstrate for the first time the spin texture of the Fermi level photoemission map measured with 6 eV photons. Previous SARPES studies only probed selected regions in the Brillouin zone (BZ) [19–21]. We further demonstrate that the symmetry of the ARPES spin texture reflects the WTe₂ surface symmetry with a single mirror plane present, and not the initial state spin symmetry. Therefore, we directly demonstrate that the ARPES photocurrent carries additional information beyond the initial band structure spin texture, due to what we call *the geometry-induced spin filtering effect*.

The results are analyzed by comparison to the dedicated theoretical DFT calculations. The results obtained within the linearized-augmented plane-wave (LAPW) scheme show that the initial state spin texture follows the expected axial vector transformation rules of a single mirror plane and time-reversal. Further one-step model photoemission calculations within the Korringa-Kohn-Rostoker (KKR) scheme reproduce the (broken) symme-

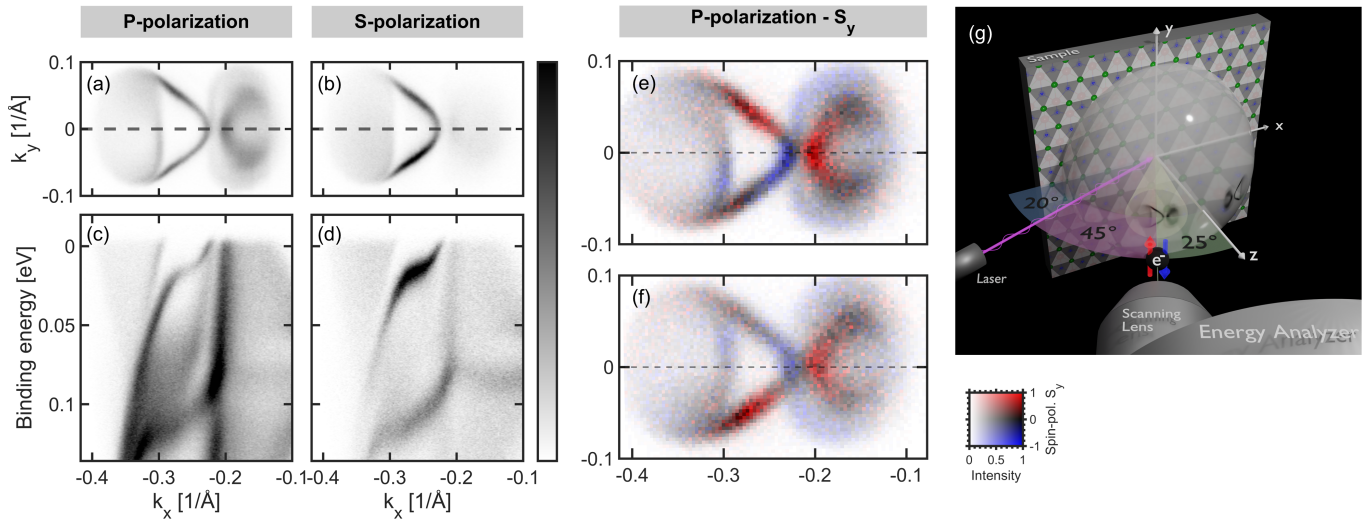


FIG. 1. (a-b) Spin-integrated laser ARPES Fermi surface maps measured with p - and s -polarized light. (c-d) Corresponding energy dispersions $E(k_x)$ for $k_y = 0$ as indicated by the dashed lines in (a) and (b). (e-f) Experimental laser-SARPES 57×89 pixel Fermi surface maps taken at two nearby spots on the same cleave. The false color scale refers to the spin polarization S_{fy} in the ensemble of the photoemitted electrons. (g) Schematic geometry of the SARPES experiment. The maps were measured using the lens deflector system collecting the emission angles indicated by the yellow cone with the sample rotated by $\theta = 25^\circ$ with respect to the lens axis using p -polarized light and probing the spin along the y axis, as defined in (g).

try properties of the experimental data. Finally, within the free-electron final state ARPES model we identify the origin of the observed asymmetries as an interference of the emission from different atomic sites.

Methods.— The sample (Td-WTe₂ single crystal, space group $Pmn2_1$, purchased from *HQ graphene*) was glued to the molybdenum sample plate by a silver-epoxy. We used p - or s -polarized light from the *LEOS Solutions* continuous wave laser with $h\nu = 6.02$ eV focused down to ~ 50 μm , the *MB Scientific A1* hemispherical electron analyzer and the exchange-scattering *Focus GmbH FER-RUM* spin detector [22]. Spectrometers based on a similar design are in operation at synchrotron light sources [23, 24]. The mirror plane of WTe₂ was aligned parallel to the entrance slit of the A1 spectrometer. The mechano-electrostatic lens deflector system of A1 allows mapping the emission angle over approx. $\pm 15^\circ$ in both k_x and k_y directions, therefore allowing for point-by-point k_x vs. k_y mapping in the spin-polarized mode without rotating the sample. All measurements were carried out at ~ 15 K at the pressure in the analyzer chamber $< 5 \times 10^{-11}$ mbar.

The initial state band structure was calculated using DFT in the generalized gradient approximation [25]. We use the full-potential LAPW method in film geometry as implemented in the FLEUR code [26]. Photoemission calculations were performed within the one-step model formalism as implemented in the fully relativistic KKR method [20, 27].

Further details on methods are provided in the Section SI of the Supplemental Material.

Results.—Figure 1(a-d) shows the high-resolution

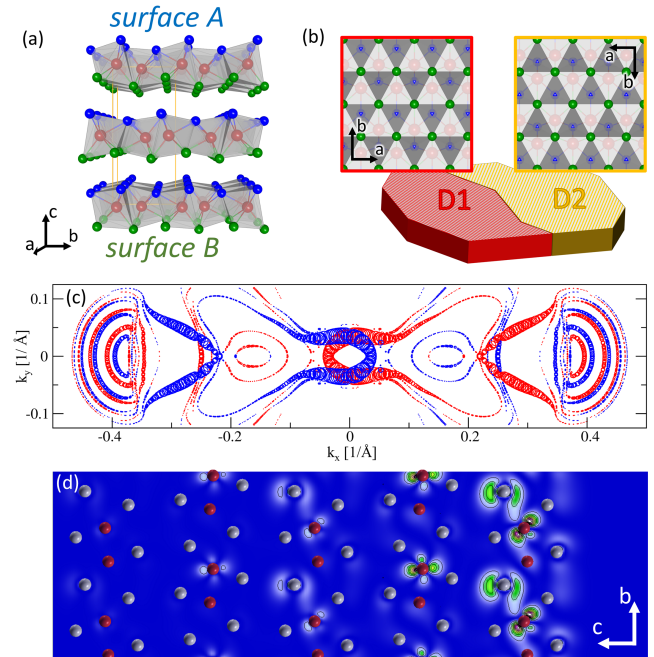


FIG. 2. Crystal geometry and initial state spin textures. (a) The 3D impression of the WTe₂ crystal structure. (b) The probed surface with two possible terminations, which we label D1 and D2. (c) The S_y component of the theoretical Fermi level spin texture, which is the same for both domains. The size of the symbols corresponds to the spin-polarization in the first layer (containing two formula units). (d) The surface state charge density in real space at $k_x = -0.3 \text{ \AA}^{-1}$ and initial energy -25 meV (see Supplemental Material Fig. S6).

ARPES maps measured with the 6 eV laser which are in quantitative agreement with previously published results [4, 16]. Figure 1(e-f) shows the spin-polarized Fermi surface maps with p -polarized light from two different spots on the sample in the off-normal geometry described in Fig. 1(g), using the A1 lens deflector system to map the important portion of the BZ without rotating the sample. The use of the deflector system is critical to assure that the entire map is taken with the laser beam focused on precisely the same spot on the sample. Both maps show the familiar shape previously reported in Refs. [4, 16], however, their spin textures are different and highly asymmetric. Supplemental Material Fig. S4 shows SARPES spin texture taken with s -polarized light, where the spin polarization asymmetry, albeit smaller, is also observed.

The crystal lattice of WTe₂ is shown schematically in Fig. 2(a-b). The surface of WTe₂ exhibits a single \mathcal{M}_x mirror plane, while the y and z directions are polar (see Section SII of the Supplemental Material and Ref. [28]). By convention, the polarity along the z axis has been defined as surface A (or *top*) and B (or *bottom*), as depicted in Fig. 2(a), with radically different Fermi contours measured on these surfaces [4, 18]. The shapes of Fermi surfaces from Fig. 1(a-b,e-f) have been associated with the surface B .

The glide-reflection operation ($1/2 + x, -y, 1/2 + z$) of the $Pmn2_1$ space group [28] shows that adjacent terraces, which we call $D1$ and $D2$, have reversed polarity along y , as shown explicitly in Fig. 2(b). Cleaved TMDCs typically exhibit macroscopically large terraces of the sizes of 100 μm or larger, and with our laser beamspot of 50 μm we can routinely address a single terrace, therefore we assume that the spectra in Fig. 1(e-f) are taken on single terraces of reversed polarity.

Since WTe₂ is non-magnetic, the spin expectation value \mathbf{S}_i of the initial state has to follow $\mathbf{S}_i(\mathbf{k}_i) = -\mathbf{S}_i(-\mathbf{k}_i)$. For the surface states, by combining this with the axial vector rules for the \mathcal{M}_x mirror plane, one gets $S_{iy}(k_{ix}, k_{iy}) = S_{iy}(k_{ix}, -k_{iy})$, and our theoretical initial state spin texture for surface B shown in Fig. 2(c) obeys this symmetry. However, this symmetry is broken in Fig. 1(e) and in 1(f). Already from the visual inspection in some portions of these SARPES maps S_{fy} changes sign between (k_{fx}, k_{fy}) and $(k_{fx}, -k_{fy})$, while in other portions it does not. Here, \mathbf{k}_f refers to the momentum and S_{fy} to the y component of the spin expectation value in the ensemble of photoemitted electrons measured by SARPES. We note that in ARPES, the component of \mathbf{k}_f parallel to the surface is related to the off-normal emission angle θ and kinetic energy E_{kin} by $k_{f\parallel} = (1/\hbar)\sqrt{2mE_{kin}}\sin\theta$ and the parallel momentum component is conserved in the photoemission process, i.e. $\mathbf{k}_{f\parallel} = \mathbf{k}_{i\parallel}$.

A visual inspection suggests that Fig. 1(e) can be transformed into Fig. 1(f) by $S_{fy}(k_{fx}, k_{fy}) \rightarrow$

$S_{fy}(k_{fx}, -k_{fy})$, which is indeed confirmed by a quantitative standard deviation analysis, see Section SI of the Supplemental Material. This can be explained by the symmetry operation ($1/2 + x, -y, 1/2 + z$) of the $Pmn2_1$ space group, assuming (e) and (f) are measured on adjacent terraces. Here the $1/2 + z$ operation indicates switching into the adjacent layer/terrace. Reciprocal methods such as ARPES are insensitive to lateral shifts of the entire lattice and therefore the $1/2$ component in the $1/2 + x$ operation can be ignored when considering the symmetries of ARPES. This means that SARPES maps from adjacent terraces are connected by the \mathcal{M}_y mirror operation. Since in our geometry neither the s -polarized nor the p -polarized light is breaking the \mathcal{M}_y mirror plane, this leads to $\mathcal{M}_y\{S_{fy}^{D1}(k_{fx}, k_{fy})\} = S_{fy}^{D2}(k_{fx}, -k_{fy})$ for our ARPES maps from adjacent terraces $D1$ and $D2$ (Fig. 2(b)).

Figure 2(d) shows that surface state on surface B is primarily localized within the first two WTe₂ monolayers. One can also recognize a complex orbital structure of the surface state, with different orbital orientations contributing within the first and the second WTe₂ layers indicating radical breaking of the \mathcal{M}_y mirror symmetry. Approximate shapes of p_z orbitals on Te atoms and d_{z^2} on W atoms can be recognized, however, they are not perfectly aligned along the z axis.

Figure 3(a-h) presents one-step model calculations of the spin-polarization from WTe₂ at our experimental parameters, and at the theoretical KKR binding energy $E_B = 0.15$ eV that best matches the experimental Fermi level (see Section SIII of the Supplemental Material for details). For both the p - and s -polarized light and for both the free-electron final state (FEFS) and time-reversed (TR) LEED final states, the S_{fy} ARPES spin textures exhibit broken \mathcal{M}_y symmetry, unlike in the initial state map in Fig. 2(c), but in qualitative agreement with the experiment. Considering the system of a sample together with an incident light, for s -polarized light the \mathcal{M}_x symmetry of the WTe₂ is conserved, because in this case the \mathbf{E} field of the light is along the y axis, leading to $S_{fy}(k_{fx}, k_{fy}) = -S_{fy}(-k_{fx}, k_{fy})$. For the p -polarized light \mathcal{M}_x is broken due to \mathbf{E} being within the xz plane.

Fig. 3 (i-m) theoretically explore the parameter space for p - and s -polarized light. While the asymmetry effect is firmly confirmed, for both polarizations it strongly depends on photon and binding energies. Furthermore, in contrast to experiment, at the experimental parameters its magnitude is predicted to be smaller for p -polarized light than for s -polarized light.

Discussion.— The origin of the spin-filtering effect can be understood within the tight-binding (TB) formalism taking into account the FEFS matrix element $w(k_{fx}, k_{fy}, k_{fy}) = \langle e^{i\mathbf{k}_f \cdot \mathbf{r}} | \psi_i(k_{ix}, k_{iy}, \mathbf{r}) \rangle$ [29, 30], where ψ_i is the initial surface state eigenfunction with an eigenvalue (binding energy) E_B . Assuming a system of N orbitals $|j\rangle$ at positions \mathbf{r}_j we can write $\psi_i(k_{ix}, k_{iy}, \mathbf{r}) =$

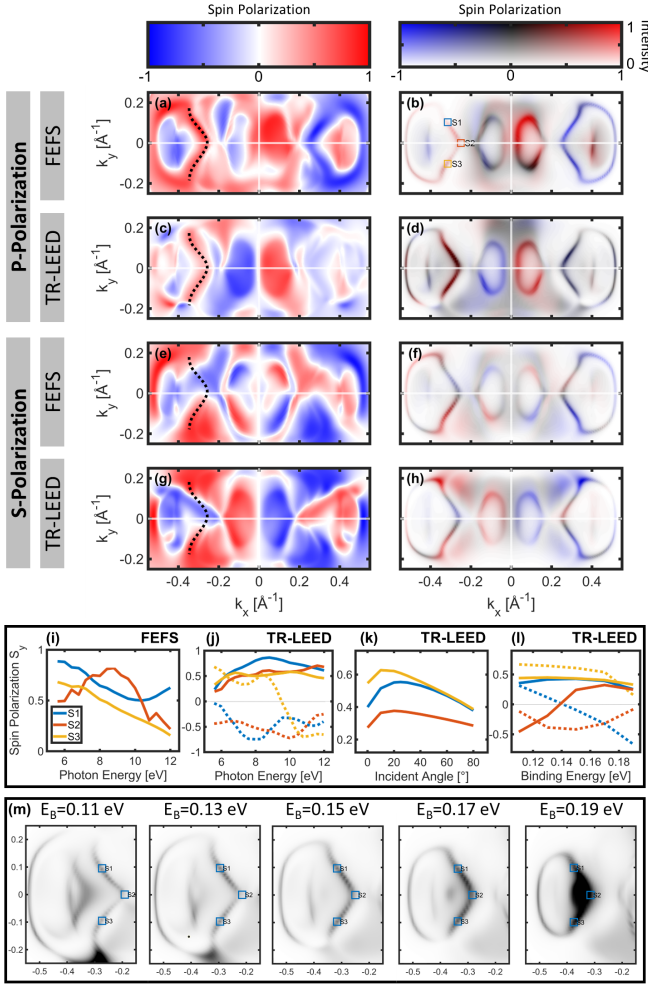


FIG. 3. One-step-model calculation of spin polarization S_y (a-d) p -polarized and (e-h) s -polarized light. (a), (c), (e) and (g) show pure spin polarization, while (b), (d), (f), and (h) are weighted by photoemission intensity. For (a-b) and (e-f) the FEFS was used, while for (c-d) and (g-h) the TR-LEED final state was used. (i-k) depict the magnitude of S_y at 3 momenta $S1$ - $S3$ indicated in (b), solid lines are for p -polarized light, and dashed lines in (j) and (l) are for s -polarized light. (i) and (j) show the dependence on photon energy for the FEFS and TR-LEED final states, respectively. (k) shows the dependence on the off-normal light incidence angle. (l) shows the dependence on binding energy for the momenta indicated in (m), where TR-LEED maps (with p -polarized light) at several binding energies are shown. For convenience the dashed lines in (a), (c), (e), and (g) indicate the location of the surface state.

$\sum_{j=1}^N C_j |j\rangle \delta(\mathbf{r} - \mathbf{r}_j)$. The FEFS matrix element is essentially a Fourier transform and therefore different sites \mathbf{r}_j will lead to phase shifts $e^{i\mathbf{k}_f \cdot \mathbf{r}_j}$. Since within the TB formalism only discrete sites \mathbf{r}_j are considered, the matrix element will have a form of a sum $w(k_{fx}, k_{fy}, k_{fz}) = \sum_{j=1}^N e^{i\mathbf{k}_f \cdot \mathbf{r}_j} C_j |j\rangle$.

Relating to squares $S1$ and $S3$ in Fig. 3(b), for a periodic system, probing initial parallel momenta $\mathbf{k}_{iS1} =$

(k_{ix}, k_{iy}) and $\mathbf{k}_{iS3} = (k_{ix}, -k_{iy})$ by ARPES requires measuring electrons emitted along $\mathbf{k}_{fS1} = (k_{ix}, k_{iy}, k_{fz})$ and $\mathbf{k}_{fS3} = (k_{ix}, -k_{iy}, k_{fz})$. For a particular photon energy $h\nu$, k_{fz} can be determined through $|\mathbf{k}_f| = (1/\hbar)\sqrt{2mE_{kin}}$, where $E_{kin} = h\nu - W - E_B$ and W is the work function, making the model $h\nu$ -dependent.

Since atomic sites are positioned such that \mathcal{M}_y is broken, this will lead to different \mathbf{r}_j -derived phase shifts in $\langle e^{i\mathbf{k}_{fS1} \cdot \mathbf{r}} | \psi_i(\mathbf{k}_{iS1}, \mathbf{r}) \rangle$ and $\langle e^{i\mathbf{k}_{fS3} \cdot \mathbf{r}} | \psi_i(\mathbf{k}_{iS3}, \mathbf{r}) \rangle$. One can show that in a generic case this leads to different spin polarizations for the two emission directions, \mathbf{k}_{fS1} and \mathbf{k}_{fS3} , despite equal initial state polarizations $S_{iy}(\mathbf{k}_{fS1})$ and $S_{iy}(\mathbf{k}_{fS3})$, as discussed earlier. A full derivation of this interference model for the minimal case of 2 orbitals on 2 different sites, that is lengthy but elementary, is presented in Section SIV of the Supplemental Material, while the complex orbital structure (Fig. 2(d)) forbids writing a realistic TB model of WTe_2 . The existence of the asymmetry for s -polarized light (Supplemental Material Fig. S4) is in agreement with the interference model and points out that the effect is not related to breaking of the \mathcal{M}_x mirror plane by the p -polarized light.

Fig. 3(i-m) illustrates sensitive dependence of the SARPES spin texture on various parameters. Importantly, the predicted effect at the experimental parameters (p -polarized light, $h\nu = 6$ eV, light incidence angle 80°) is small, which calls for further improvement of the theoretical description that is critical in establishing whether WTe_2 realizes a Weyl type-II phase. These improvements can include further exploring correlation effects [14], and structural changes [18, 31] and relaxations, which can lead to significant renormalization of the electronic structure and orbital character of the surface states.

In this spirit, we propose that establishing initial state spin textures experimentally shall involve iterative optimization of the agreement to the initial state and one-step model calculations, exploring the parameter space such as in Fig. 3(i-m). Experimentally this is currently challenging, but might be feasible using the new generation spin detectors [32, 33].

Following the above arguments, we propose that spin asymmetries as observed here shall be present in SARPES from every surface that exhibits spin-momentum locked spin-polarized bands and lacks the mirror plane perpendicular to one of the lateral directions. Previously similar effects have been studied theoretically, but not directly discussed, for topological insulators [30] and Rashba systems [34].

The presented effect is different from the interference photoemission models for the generic orientation of the light polarization [35], since these models do not take into account phase shifts in matrix element due to different locations of atomic sites. Spin filtering in photoemission through ultrathin ferromagnetic layers has been discussed previously [36], however, the effect in WTe_2 is

different since it does not involve time-reversal symmetry breaking in the initial state. Conversely, a filtering due to non-magnetic overlayers on magnetic substrates has also been studied [37], which is again different from the effect discussed here, since it involves a modification of the initial band structure.

Summary.— Low crystal symmetry of WTe_2 , which is responsible for its exotic transport properties, leads to emerging asymmetries in the SARPES spin textures. We have characterized spin textures in the photoelectron ensemble from WTe_2 surfaces excited by the 6 eV continuous wave laser light. Despite the overall high asymmetry, the spin textures of adjacent terraces are connected by the \mathcal{M}_y mirror symmetry operation. Results have been obtained using a novel SARPES machine that enables 2D mapping of the spin textures with reduced instrumental asymmetries. The modulation of the photoelectron spin-polarization can be interpreted as the geometry-induced, light-polarization-independent spin filtering effect which can be modeled qualitatively within the free-electron final state photoemission model with the $\langle e^{i\mathbf{k}\cdot\mathbf{r}} | \psi(\mathbf{k}, \mathbf{r}) \rangle$ matrix element.

These results are the first demonstration of the surface spin texture of WTe_2 over the extended momentum range, and demonstrate a new aspect of a non-trivial connection between the initial state band structure properties and the photoelectron constant energy reciprocal space maps. Similar effects are expected in other quantum materials where a corresponding experimental geometry can be established. A more complete picture could be obtained by combining circular-dichroic and spin-texture ARPES maps which could address the orbital character of the participating states towards the identification of the transport-relevant Berry curvature hot spots. In this way, our results call for future research to establish a possible connection to the spin transport of hot electrons inside the crystal, through the interfaces, and through the surface barrier.

Authors would like to thank F. Freimuth, D. Nabok, S. Ghosh, J. Henk and Ph. Rüßmann for fruitful discussions. Moreover, L. P. and T. H. acknowledge the support of Peter Baltzer (MB Scientific), Nicola Gatti (LEOS Solutions), and Matthias Escher (Focus GmbH). At different stages of this project the position of T. H. was funded by the Deutsche Forschungsgemeinschaft (DFG, German Research Foundation) under Germany's Excellence Strategy – Cluster of Excellence Matter and Light for Quantum Computing (ML4Q) EXC 2004/1 – 390534769 and by the DFG Priority Program SPP1666. J. M. and J. S. would like to thank the CEDAMNF (Grant No. CZ.02.1.01/0.0/0.0/15_003/0000358) co-funded by the Ministry of Education, Youth and Sports of Czech Republic and the GACR Project No. 20-18725S for funding. J. S. and F. R. acknowledge financial support from the DFG through the Würzburg-Dresden Cluster of Excellence on Complexity and Topology in Quantum

Matter – *ct.qmat* (EXC 2147, project-id 39085490). G. B. gratefully acknowledges the computing time granted through JARA-HPC on the supercomputer JURECA at Forschungszentrum Jülich.

* l.plucinski@fz-juelich.de

- [1] M. N. Ali, J. Xiong, S. Flynn, J. Tao, Q. D. Gibson, L. M. Schoop, T. Liang, N. Haldolaarachchige, M. Hirschberger, N. P. Ong, and R. J. Cava, Large, non-saturating magnetoresistance in WTe_2 , *Nature* **514**, 205 (2014).
- [2] A. A. Soluyanov, D. Gresch, Z. Wang, Q. Wu, M. Troyer, X. Dai, and B. A. Bernevig, Type-II weyl semimetals, *Nature* **527**, 495 (2015).
- [3] P. Rüßmann, A. P. Weber, F. Glott, N. Xu, M. Fanciulli, S. Muff, A. Magrez, P. Bugnon, H. Berger, M. Bode, J. H. Dil, S. Blügel, P. Mavropoulos, and P. Sessi, Universal scattering response across the type-ii weyl semimetal phase diagram, *Phys. Rev. B* **97**, 075106 (2018).
- [4] F. Y. Bruno, A. Tamai, Q. S. Wu, I. Cucchi, C. Barreteau, A. de la Torre, S. McKeown Walker, S. Riccò, Z. Wang, T. K. Kim, M. Hoesch, M. Shi, N. C. Plumb, E. Giannini, A. A. Soluyanov, and F. Baumberger, Observation of large topologically trivial fermi arcs in the candidate type-ii weyl semimetal WTe_2 , *Phys. Rev. B* **94**, 121112 (2016).
- [5] S. Tang, C. Zhang, D. Wong, Z. Pedramrazi, H.-Z. Tsai, C. Jia, B. Moritz, M. Claassen, H. Ryu, S. Kahn, J. Jiang, H. Yan, M. Hashimoto, D. Lu, R. G. Moore, C.-C. Hwang, C. Hwang, Z. Hussain, Y. Chen, M. M. Ugeda, Z. Liu, X. Xie, T. P. Devereaux, M. F. Crommie, S.-K. Mo, and Z.-X. Shen, Quantum spin hall state in monolayer $1t'$ - WTe_2 , *Nature Physics* **13**, 683 (2017).
- [6] V. Fatemi, S. Wu, Y. Cao, L. Bretheau, Q. D. Gibson, K. Watanabe, T. Taniguchi, R. J. Cava, and P. Jarillo-Herrero, Electrically tunable low-density superconductivity in a monolayer topological insulator, *Science* **362**, 926 (2018), <https://science.sciencemag.org/content/362/6417/926.full.pdf>.
- [7] E. Sajadi, T. Palomaki, Z. Fei, W. Zhao, P. Bement, C. Olsen, S. Luescher, X. Xu, J. A. Folk, and D. H. Cobden, Gate-induced superconductivity in a monolayer topological insulator, *Science* **362**, 922 (2018), <https://science.sciencemag.org/content/362/6417/922.full.pdf>.
- [8] I. Sodemann and L. Fu, Quantum nonlinear hall effect induced by berry curvature dipole in time-reversal invariant materials, *Phys. Rev. Lett.* **115**, 216806 (2015).
- [9] Q. Ma, S.-Y. Xu, H. Shen, D. MacNeill, V. Fatemi, T.-R. Chang, A. M. M. Valdivia, S. Wu, Z. Du, C.-H. Hsu, S. Fang, Q. D. Gibson, K. Watanabe, T. Taniguchi, R. J. Cava, E. Kaxiras, H.-Z. Lu, H. Lin, L. Fu, N. Gedik, and P. Jarillo-Herrero, Observation of the nonlinear hall effect under time-reversal-symmetric conditions, *Nature* **565**, 337 (2019).
- [10] K. Kang, T. Li, E. Sohn, J. Shan, and K. F. Mak, Non-linear anomalous hall effect in few-layer WTe_2 , *Nature Materials* **18**, 324 (2019).
- [11] Z. Z. Du, H.-Z. Lu, and X. C. Xie, Nonlinear hall effects, *Nature Reviews Physics* 10.1038/s42254-021-00359-6 (2021).

- [12] I. Pletikosić, M. N. Ali, A. V. Fedorov, R. J. Cava, and T. Valla, Electronic structure basis for the extraordinary magnetoresistance in wte_2 , *Phys. Rev. Lett.* **113**, 216601 (2014).
- [13] Y. Wu, N. H. Jo, M. Ochi, L. Huang, D. Mou, S. L. Bud'ko, P. C. Canfield, N. Trivedi, R. Arita, and A. Kaminski, Temperature-induced lifshitz transition in wte_2 , *Phys. Rev. Lett.* **115**, 166602 (2015).
- [14] D. Di Sante, P. K. Das, C. Bigi, Z. Ergönenc, N. Gürtler, J. A. Krieger, T. Schmitt, M. N. Ali, G. Rossi, R. Thomale, C. Franchini, S. Picozzi, J. Fujii, V. N. Strocov, G. Sangiovanni, I. Vobornik, R. J. Cava, and G. Panaccione, Three-dimensional electronic structure of the type-II Weyl semimetal wte_2 , *Phys. Rev. Lett.* **119**, 026403 (2017).
- [15] A. B. Pippard, *Magnetoresistance in metals* (Cambridge University Press, Cambridge England New York, 1989).
- [16] C.-L. Wang, Y. Zhang, J.-W. Huang, G.-D. Liu, A.-J. Liang, Y.-X. Zhang, B. Shen, J. Liu, C. Hu, Y. Ding, D.-F. Liu, Y. Hu, S.-L. He, L. Zhao, L. Yu, J. Hu, J. Wei, Z.-Q. Mao, Y.-G. Shi, X.-W. Jia, F.-F. Zhang, S.-J. Zhang, F. Yang, Z.-M. Wang, Q.-J. Peng, Z.-Y. Xu, C.-T. Chen, and X.-J. Zhou, Evidence of electron-hole imbalance in WTe_2 from high-resolution angle-resolved photoemission spectroscopy, *Chinese Physics Letters* **34**, 097305 (2017).
- [17] Y. Wu, N. H. Jo, D. Mou, L. Huang, S. L. Bud'ko, P. C. Canfield, and A. Kaminski, Three-dimensionality of the bulk electronic structure in wte_2 , *Phys. Rev. B* **95**, 195138 (2017).
- [18] A. Rossi, G. Resta, S. H. Lee, R. D. Redwing, C. Jozwiak, A. Bostwick, E. Rotenberg, S. Y. Savrasov, and I. M. Vishik, Two phase transitions driven by surface electron doping in wte_2 , *Phys. Rev. B* **102**, 121110 (2020).
- [19] B. Feng, Y.-H. Chan, Y. Feng, R.-Y. Liu, M.-Y. Chou, K. Kuroda, K. Yaji, A. Harasawa, P. Moras, A. Barinov, W. Malaeb, C. Bareille, T. Kondo, S. Shin, F. Komori, T.-C. Chiang, Y. Shi, and I. Matsuda, Spin texture in type-II Weyl semimetal wte_2 , *Phys. Rev. B* **94**, 195134 (2016).
- [20] M. Fanciulli, J. Schusser, M.-I. Lee, Z. E. Youbi, O. Heckmann, M. C. Richter, C. Cacho, C. Spezzani, D. Bresteau, J.-F. m. c. Hergott, P. D'Oliveira, O. Tcherbakoff, T. Ruchon, J. Minár, and K. Hrivcovini, Spin, time, and angle resolved photoemission spectroscopy on wte_2 , *Phys. Rev. Research* **2**, 013261 (2020).
- [21] Y. Wan, L. Wang, K. Kuroda, P. Zhang, K. Koshiishi, M. Suzuki, J. Kim, R. Noguchi, C. Bareille, K. Yaji, A. Harasawa, S. Shin, S.-W. Cheong, A. Fujimori, and T. Kondo, Selective observation of surface and bulk bands in polar wte_2 by laser-based spin- and angle-resolved photoemission spectroscopy, *Phys. Rev. B* **105**, 085421 (2022).
- [22] M. Escher, N. B. Weber, M. Merkel, L. Plucinski, and C. M. Schneider, Ferrum: A new highly efficient spin detector for electron spectroscopy, *e-J. Surf. Sci. Nanotech.* **9**, 340 (2011).
- [23] T. Okuda, Y. Takeichi, Y. Maeda, A. Harasawa, I. Matsuda, T. Kinoshita, and A. Kakizaki, A new spin-polarized photoemission spectrometer with very high efficiency and energy resolution, *Review of Scientific Instruments* **79**, 123117 (2008), <https://doi.org/10.1063/1.3058757>.
- [24] C. Bigi, P. K. Das, D. Benedetti, F. Salvador, D. Krizmančić, R. Sergo, A. Martin, G. Panaccione, G. Rossi, J. Fujii, and I. Vobornik, Very efficient spin polarization analysis (VESPA): new exchange scattering-based setup for spin-resolved ARPES at APE-NFFA beamline at Elettra, *Journal of Synchrotron Radiation* **24**, 750 (2017).
- [25] J. P. Perdew, K. Burke, and M. Ernzerhof, Generalized gradient approximation made simple, *Phys. Rev. Lett.* **77**, 3865 (1996).
- [26] FLEUR, <http://www.flapw.de/>.
- [27] J. Braun, J. Minár, and H. Ebert, Correlation, temperature and disorder: Recent developments in the one-step description of angle-resolved photoemission, *Physics Reports* **740**, 1 (2018), correlation, temperature and disorder: Recent developments in the one-step description of angle-resolved photoemission.
- [28] A. P. Weber, P. Rüßmann, N. Xu, S. Muff, M. Fanciulli, A. Magrez, P. Bugnon, H. Berger, N. C. Plumb, M. Shi, S. Blügel, P. Mavropoulos, and J. H. Dil, Spin-resolved electronic response to the phase transition in $mote_2$, *Phys. Rev. Lett.* **121**, 156401 (2018).
- [29] S. Moser, An experimentalist's guide to the matrix element in angle resolved photoemission, *Journal of Electron Spectroscopy and Related Phenomena* **214**, 29 (2017).
- [30] Z.-H. Zhu, C. N. Veenstra, G. Levy, A. Ubaldini, P. Syers, N. P. Butch, J. Paglione, M. W. Haverkort, I. S. Elfimov, and A. Damascelli, Layer-by-layer entangled spin-orbital texture of the topological surface state in bi_2se_3 , *Phys. Rev. Lett.* **110**, 216401 (2013).
- [31] J. Xiao, Y. Wang, H. Wang, C. D. Pemmaraju, S. Wang, P. Muscher, E. J. Sie, C. M. Nyby, T. P. Devereaux, X. Qian, X. Zhang, and A. M. Lindenberg, Berry curvature memory through electrically driven stacking transitions, *Nature Physics* **16**, 1028 (2020).
- [32] C. Tusche, A. Krasnyuk, and J. Kirschner, Spin resolved bandstructure imaging with a high resolution momentum microscope, *Ultramicroscopy* **159**, 520 (2015), special Issue: LEEM-PEEM 9.
- [33] G. Schönhense, K. Medjanik, and H.-J. Elmers, Space-, time- and spin-resolved photoemission, *Journal of Electron Spectroscopy and Related Phenomena* **200**, 94 (2015), special Anniversary Issue: Volume 200.
- [34] H. Bentmann, H. Maaß, E. E. Krasovskii, T. R. F. Peixoto, C. Seibel, M. Leandersson, T. Balasubramanian, and F. Reinert, Strong linear dichroism in spin-polarized photoemission from spin-orbit-coupled surface states, *Phys. Rev. Lett.* **119**, 106401 (2017).
- [35] K. Yaji, K. Kuroda, S. Toyohisa, A. Harasawa, Y. Ishida, S. Watanabe, C. Chen, K. Kobayashi, F. Komori, and S. Shin, Spin-dependent quantum interference in photoemission process from spin-orbit coupled states, *Nature Communications* **8**, 10.1038/ncomms14588 (2017).
- [36] J. Henk, P. Bose, T. Michael, and P. Bruno, Spin motion of photoelectrons, *Phys. Rev. B* **68**, 052403 (2003).
- [37] T. Berdot, A. Hallal, L. T. Bismaths, L. Joly, P. Dey, J. Henk, M. Alouani, and W. Weber, Effect of submonolayer mgo coverages on the electron-spin motion in $fe(001)$: Experiment and theory, *Phys. Rev. B* **82**, 172407 (2010).